INTERNATIONAL ATOMIC ENERGY AGENCY
UNITED NATIONS EDUCATIONAL, SCIENTIFIC AND CULTURAL ORGANIZATION

INTERNATIONAL CENTRE FOR THEORETICAL PHYSICS
34100 TRIESTE (ITALY) - P.O.B. 586 - MIRAMARE - STRADA COSTIERA 11 - TELEPHONES: 224281/2/3/4/5/6
CABLE: CENTRATOM - TELEX 460392 - I

H4.SMR/164 - 08

WORKSHOP ON CLOUD PHYSICS AND CLIMATE

23 November - 20 December 1985

REMOTE SENSING SATELLITE AND RADAR METEOROLOGY - II

G. DUGDALE

Dept. of Meteorology
Univ. of Reading
U.K.

7 - FURTHER APPLICATIONS OF SATELLITE DATA IN METEOROLOGY

7.1 Wind finding

7.1.1. Tropospheric winds

Over the oceans the tracking of clouds in either or both the visible and thermal infra-red channels offers a ready means of assessing wind speeds. It is assumed that the clouds are moved by the wind at about the level of their tops. This level is determined from the cloud top temperature and climatic or synoptic data about the atmospheric temperature profile. Many schemes involving automated or manual pattern recognition techniques have been developed for calculating satellite cloud tracking, most involve interactive image processing. A fairly typical method is outlined below.

Figure 7.1.

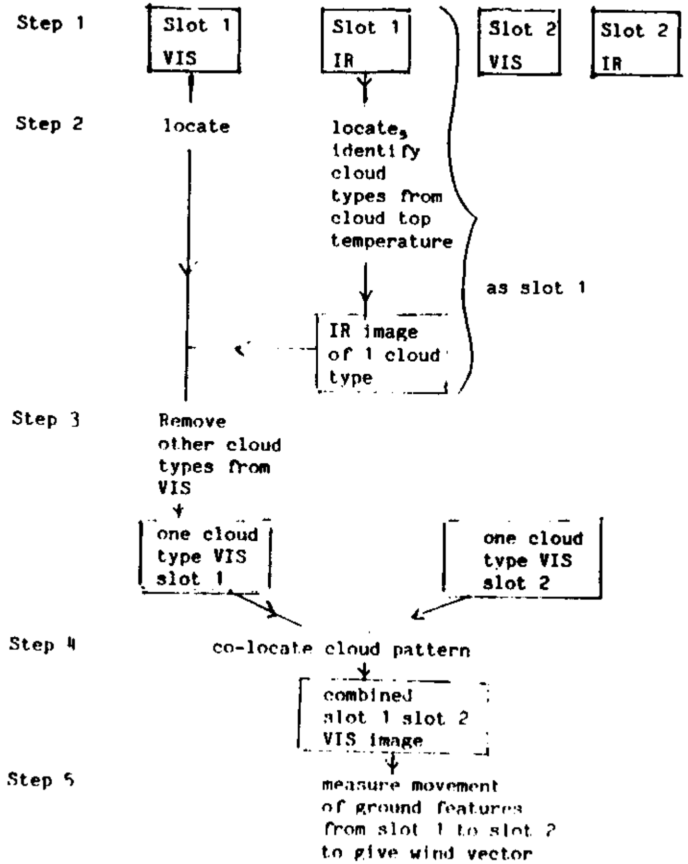

Steps 3 to 5 are repeated for each cloud level present.

Areas of about 1° square are treated at a time. Low level winds from stratocumulus or cumulus cloud movement have standard errors of about 1.5 m s^{-1} while high level winds from cirrus tracking give errors of about 2.0 m s^{-1}.

7.1.2. Surface wind

Satellite borne radar has been used in an experimental mode to measure surface winds over the ocean. The SEASAT-A scatterometer system (SASS) detects the small scale roughness of the ocean surface from the increased radar back scattering, the change in polarization and the doppler shift of the back scattered signal indicate the direction of the wind relative to the satellite. The surface roughness is correlated with the wind speed empirically. Results indicate that winds may be measured to ± 2.0 m s^{-1} in strength and to ± 20° in direction.

7.2 Rainfall estimation from satellite data

7.2.1. Microwave techniques

The most promising technique for rainfall estimation is the, as yet experimental, one using microwave emission to detect the presence of liquid water in clouds.

7.2.2. Infra-red and visible techniques

As there is at present no commitment for operational meteorological satellites with microwave channels suitable for rainfall estimation. Methods using the currently available visible and thermal infra-red channels have been developed experimentally and have had limited operational use.

These methods rely on recognising the thermal I-R and VIS imagery the main characteristics of rain producing cloud systems. Large liquid water content gives rise to high reflectance in the visible channel and clouds reaching high levels in the atmosphere such as cumulonimbus can be recognised in the thermal I.R.

Figures 7.2. a, b, and c below illustrate these characterics.

Fig.7.2. Joint frequency distribution [illegible] for a 400 x 400 km box centred at [illegible] Atlantic Ocean, 1300 GMT 5 September [illegible] tropical a scale 0-1. (a) No rain [illegible] been normalized to [illegible] Lovejoy and Austin, 1979 [illegible] After (a) and (b).

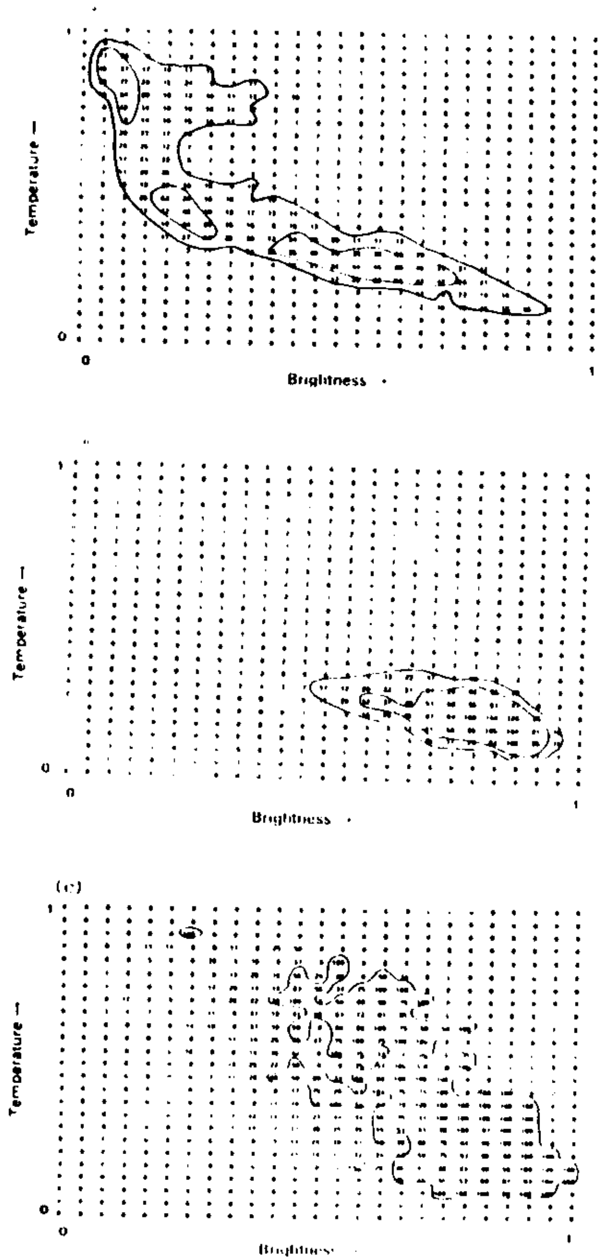

The interpretation of the clouds VIS and/or I.R. features in terms of rainfall has followed two principle lines. First, the use of high quality photographic type imagery to recognise typical rain bearing systems and to attribute rainfall amounts to them according to their persistance over an area and the climatologically expected rainfall from such systems. These methods have achieved some success particularly when used as interpolation schemes between raingauges and when applied to large scale synoptic rainfall events which give rise to relatively homogeneous rainfall at the ground. The second method, more suitable for convective rainfall, consists of monitoring the development of clouds using digital I-R data sometimes in conjunction with the visible data. It is found that convective systems give most of their rainfall in their growth stage and that having reached their maximum horizontal extent generally give little precipitation. Figure 7.3. below illustrates this.

Fig. 7.3. The area of rain producing cloud (A_e) a function of the size of the cloud (A). Both scales are normalized by the maximum size the cloud attains (A_m). The curves represent clouds of three different size ranges. (after Barrett and Martin, 1981).

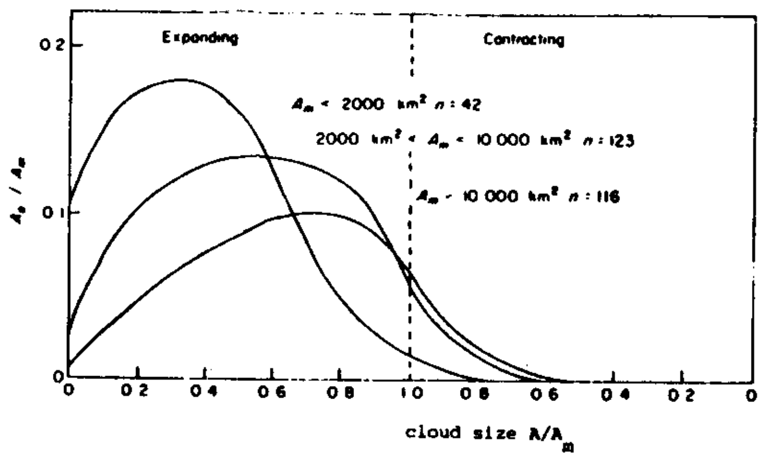

The implication of the above is that convective systems must be monitored each hour or so if reasonable estimates of rainfall from them are to be made. Hence, data from geostationary satellites must be used. Only the I-R channel can monitor their activity during the night. Most experimental and quasi-operational models employ a rainrate (R) equation of the form:

$$R = a_0 + a \frac{\partial A}{\partial t} \frac{1}{A} + \text{additional terms}$$

where a_0 implies the presence of cold cloud below a predetermined temperature (temperatures from 223 K to 243 K have been used) and $\frac{\partial A}{\partial t} \frac{1}{A}$ is the rate of growth of the area of cloud below that or another predetermined temperature. The additional terms may include such factors as storm propogation or decay. All these schemes are empirical and the coeficients established for one climatic region are not universally applicable; for instance those developed for convective storms over the tropical Atlantic Ocean proved inappropriate over continental West Africa.

Estimates of rainfall from tropical convective systems over long periods (30 days) or over large areas may be achieved without the inclusion of the growth term in the above equation. One is then left with the rainfall being related to the persistance of clouds of convective origin over a site or the mean fractional cover over an area. The implication is that, in the absence of orographic effects, when averaged over a number of rainfall events a site would experience some storms in each phase of growth or decay. Figure 7.4. shows a contingency table for the rainfall and persistance of cold cloud over sites in the Republic of Niger in

Figure 7.4.

Histogram of occurrence of rainfall at 109 rainfall stations in the Republic of Niger during July 1985. Figures in the body of the diagram indicate the duration of cold cloud (<- 60 °C) at each station receiving the range of rainfall indicated.

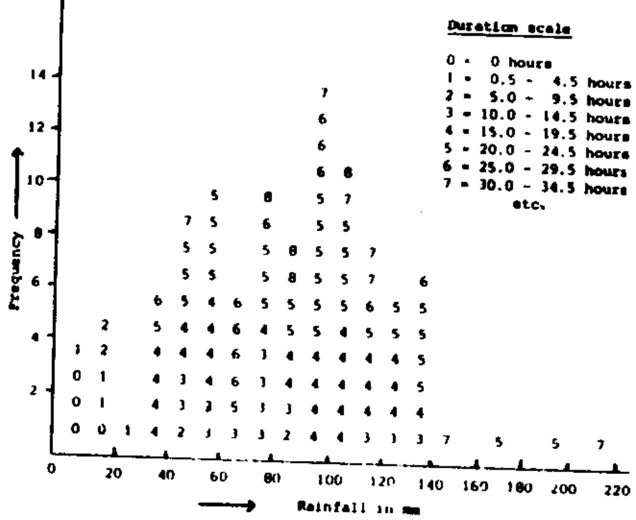

In interpretting such diagrams it is necessary to recall the large spatial variability of rainfall from these storm systems. Typically rainfall from large systems will vary by a factor of two over distances of ten kilometers. Hence raingauge data can only be used in a statistical sense to calibrate satellite estimates and similarly a satellite estimate that gave an accurate mean rainfall over a 5 km x 5 km pixel would have to be interpretted in terms of a widely spread rainfall distribution within that pixel.

7.3. Soil moisture and evaporation measurement from satellite data

Techniques for the estimation of soil moisture and evaporation from satellite data are generally based on surface energy budget (SEB) concepts and involve the use of both satellite and surface data.

The SEB may be written

$$R_N = H + \lambda E + G$$

- R_N: net radiation towards the surface
- H: sensible heat flux from the surface
- λE: evaporative heat flux from the surface
- G: ground heat flux from the surface

with

$$R_N = S(1-\alpha) + L\downarrow - L\uparrow$$

- $S(1-\alpha)$: absorbed solar radiation
- $L\downarrow$: downwards long wave radiation
- $L\uparrow$: upwards long wave radiation

The solar radiative term may be estimated from the visible channel data using climatological data for the atmospheric absorption loss. The long wave radiative terms can be calculated from satellite measured atmospheric and surface temperatures. If clouds are present cloud base temperatures must be estimated.

The heat flux terms are usually expressed in resistance terminology

$$H = \rho c_p \frac{T_s - T_a}{r_a} \quad ; \quad \lambda E = \frac{\rho c_p}{\gamma} \frac{(e_s - e_a)}{r_a}$$

$$G = k \frac{\partial T}{\partial z}\Big|_{z=0} \text{ with } c\frac{\partial T}{\partial t} = \frac{\partial}{\partial z}\left(k \frac{\partial T}{\partial z}\right) \text{ in the soil}$$

where r_a is an aerodynamic resistance which depends on wind speed and vertical temperature gradient, k is the thermal conductivity of the soil and C its volumetric thermal capacity. C is slightly dependant on soil moisture content and k strongly dependant.

If surface synoptic data (T_a, e_a, u_a) are available H may be calculated. The vapour pressure at the gound surface (e_s) is not usually known but it may be related empirically to the saturated vapour pressure at the earth surface and the difference in temperature between the surface and the air. Another approach to the λ E term is to express it as

$$\lambda E = \frac{\rho c_p}{\gamma} \frac{(e_s - e_a)}{r_a + r_\delta}$$

where δ is the depth below the soil surface at which water is available for evaporation, e_δ is then the saturated water vapour pressure at the temperature corresponding to that depth. Models to solve these equations using up to twentyfour data points per day have been developed. Other models assume all changes to be cyclic and use only two data points per day. Over bare soils with high insolution evaporation is controlled almost entirely by the resistance to vapour diffusion through the dry upper layer of soil. Under these conditions for a specified type of soil the diurnal range of surface temperature reflects well the depth of the dry layer and hence the availability of water for evaporation.

Figure 7.5 illustrates the effect on the diurnal range of temperature of a bare soil surface of irrigation and shows the rate of recovery of the temperature cycle towards the dry condition as water evaporates through the upper layers. This is the basis of one method for the estimation of soil moisture in the upper layers and of evaporation from satellite data.

Fig. 7.5.

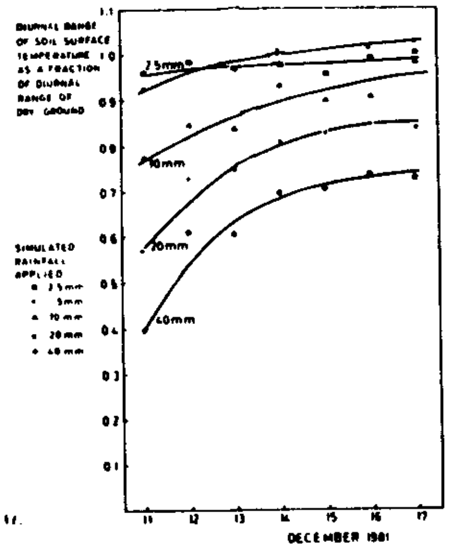

There are at present at least six models being tested for evaporation and soil moisture monitoring but none appear to have yet reached an operationally viable state.

10 - SOME OTHER APPLICATIONS OF RADAR

There are many examples of the use of radar in cloud physics and turbulence research. In this section two examples of research with radar are given. They are chosen because of the interesting novel techniques which are applied.

10.1 Radar wind finding in convective storms

Wind fields in clouds are very difficult to determine unless some components of the cloud itself can be used as tracers. Various methods, using two or more doppler radars, have been devised to investigate circulation patterns in storms. One using the "COPLAN" technique is given below.

Two doppler radars on a base line fifty to one hundred kilometers long are used to view the same section of a storm simultaneously and the velocity of the raindrops towards each radar is determined from the doppler shift.

The geometry is illustrated below

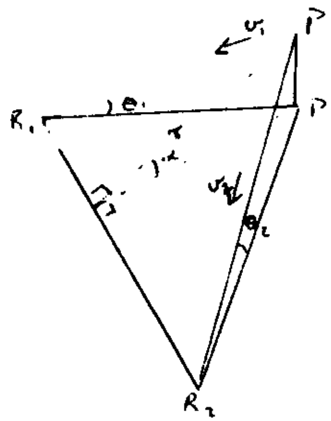

R_1, R_2 radars

P section of cloud being observed

P' plan position of P

θ_1, θ_2 elevations of P from R_1 R_2

1, 2 doppler velocities towards R_1 R_2

r the radial distance from P to R_1 R_2 making α to the horizontal

The doppler velocities v_1, v_2 contain a component from the fall speed of the drops. This may be deduced from empirical relationships between Z and the terminal velocity. One such after Atlas et al (1973) is

$$w = 2.65 Z^{0.114} (\rho_0/\rho)^{0.4} \text{ m s}^{-1} \text{ where}$$

w is the population mean terminal velocity and ρ is air density. The Doppler velocities are adjusted to v_1', v_2' where $v' = v + w \sin\theta$

From v_1', v_2' two components of the air velocity at P_1 the plane r, R_1 R_2. For ease of computation the components along and perpendicular to r are used. A series of wind fields are measured in planes containing R_1 R_2. The equation of continuity in a cylindrical co-ordinate system is then used to establish the three dimensional wind field which is then transformed to more conventionall horizontal and vertical co-ordinates. Boundary conditions are zero vertical component at the tropopause and ground surface.

The result of a storm study by Brandes and Johnson* using these methods is illustrated in Figure 10.1

* Reported by Douiak and Zrnic (1984), Doppler Radar and Weather Observations, Academic Press.

Figure 10.1. (a) Contours of reflectivity factor (in dBZ) and the storm relative wind field in a horizontal cross section at 2 km above ground level and (c) a vertical cross section of a tornadic thunderstorm on 2 May 1979, at 16:58 C.S.T. Winds are in the coordinate system moving with the storm. Storm motion speed and direction are shown. Line AB in (a) is the location of the vertical cross section. Distances are from a radar at Roman Nose State Park, Oklahoma (Alberty et al., 1979). The star pinpoints the tornado location in (a). The arrow of indicated velocity at the top right of each plot gives the speed which is proportional to the arrow's length. (From E. Brandes and D. Johnson, NSSL, personal communication.)

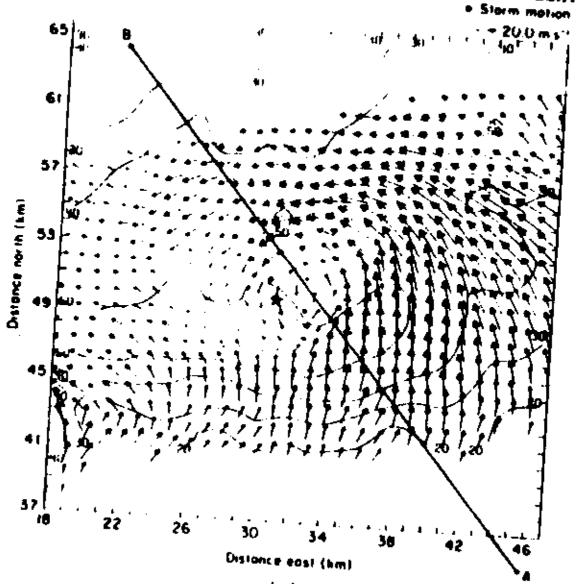

(a)

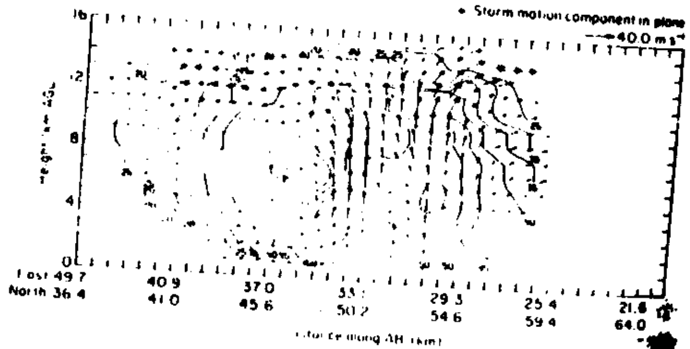

(b)

10.2 Radar on satellites

Two problems of satellite borne radar arise from the large distances between the radar and the target. The maximum resolution ($\frac{1.22\lambda}{D}$) means that for a satellite even with a ten metre antenna the ground resolution would be of the order of 10 km for a satellite orbitting at 1000 km and several hundred kilometers for a geostationary satellite. The second difficulty is that of the return power available. With an orbitting satellite the received power is only about 10^{-23} of the transmitted power which is itself much lower than the power transmitted from ground based radar.

Interesting solutions to these difficulties were found on the Synthetic Aperture Radar (SAR).

This radar viewed the earth's surface obliquely at right angles to the direction of travel of the satellite.

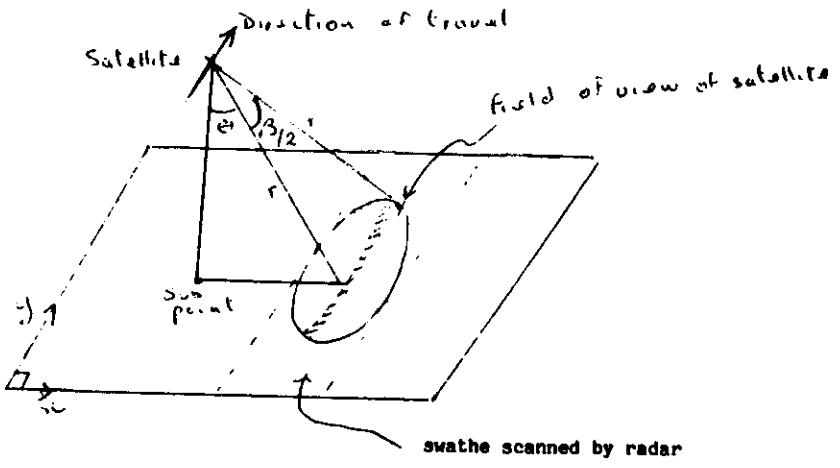

Resolution in the x direction depends on and on the pulse length, and equals ($\frac{\text{pulse length}}{2\cos\theta}$). In the y direction the resolution is $r \sin\beta$

For many purposes neither the x nor the y resolution as described above are adequate.

When a pulse is transmitted and received its power/time curve may resemble

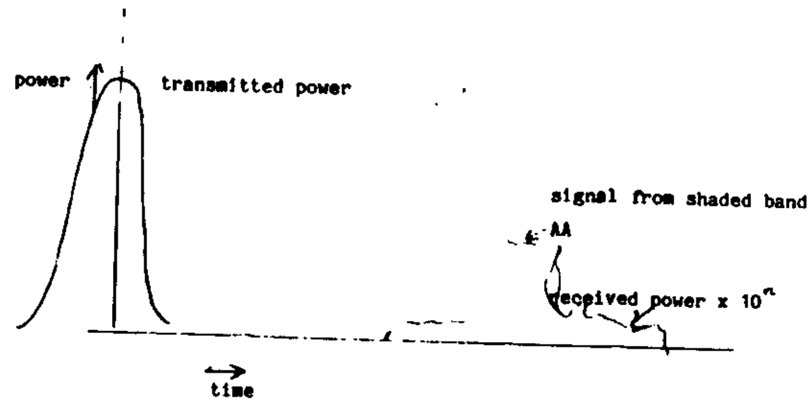

In the SAR both the received power and the x direction resolution are increased by coding the pulse signal by changing its frequency slightly throughout the duration of the pulse.

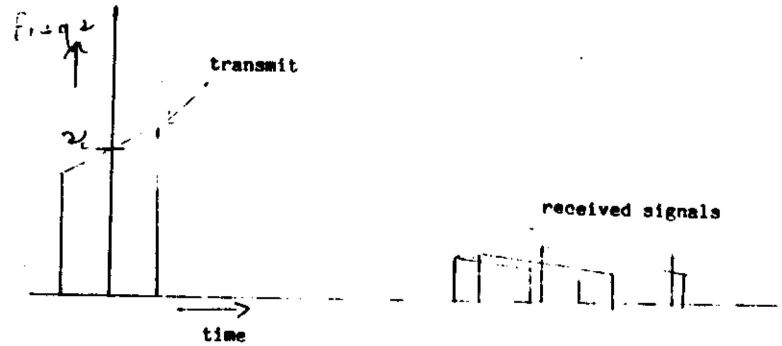

The received signal is then delayed according to its frequency so the whole pulse is compressed after reception, thus increasing power and resolution. This technique is known as the CHIRP.

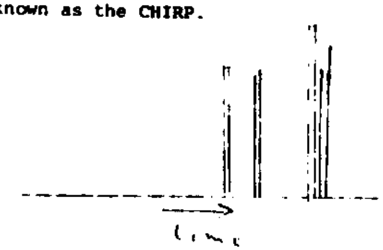

The synthetic aperture method increases the y resolution. The principle is that if a series of identical pulses and echoes are emitted and received by a moving antenna it is possible to recombine the received data as though all the pulses had been emitted simultaneously by a large antenna. The limit of the principle is that any surface point must receive at least two pulses. Hence we have the paradox that the smaller the actual antenna the larger in principle is the resolving power of the synthetic aperture. In fact power considerations giver a lower limit to the antenna size. The higher the pulse repetition frequency (P.R.F.) the more pulses will give information on any one point but the P.R.F. must not be so high that back scatter from two sources could be confused.

A simple analysis of the geometry of the SAR principle is given below.

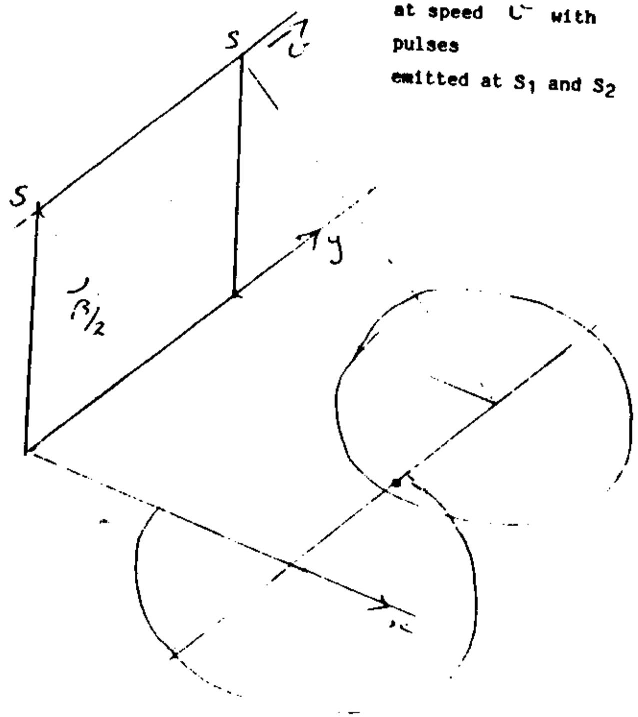

Satellite moving in direction y at speed v with pulses emitted at S_1 and S_2

The size of the synthetic aperture (A_s) may be considered to be the size of the "footprint" in the y direction = $r\beta$

with $\beta = \frac{1.22\lambda}{A_r}$ where Ar is the effective aperture of the actual antenna

So $A_s = \frac{1.22 r \lambda}{A_r}$

and the angular resolution β_s of the synthetic aperature is given by

$$\beta_s = \frac{1.22\lambda A_r}{1.22 r \lambda} = \frac{A_r}{r}$$

and the linear resolution is Ar.

This is perhaps more easily seen if one considers that the only unique information about the position of a point in the y direction is its doppler shift. The maimum doppler shift is given by

$$\Delta\nu = 2\nu_0 \frac{v\beta}{c}$$

and for two close points the maximum difference in frequencies of the return signal is given by

$$\Delta F = 2\nu_0 \frac{v}{c} \frac{\Delta p}{r}$$

where Δp is the y separation of the points

if Δp is the minimum resolvable distance the angular resolution is

$$\Delta p = \frac{r \Delta F c}{2\nu_0 v}$$

$$= \frac{r \Delta F \lambda_0}{v}$$

$$= \frac{T \Delta F \lambda_0}{\beta}$$

$$\approx T \Delta F A_r$$

where T is the time during which a point remains in view of the satellite

but the minimum resolvable frequency is $1/T$ so the linear resolution is Ar. The pulse repetition frequency limits are that a point must remain in view for more than two pulses

i.e. min P.R.F. $> \frac{v}{A_r}$

Also for signals to be unambiguous the P.R.F. $< \frac{c}{2r}$